Adsorption of CO_2, CH_4, and N_2 in Activated Carbon Honeycomb Monolith

Rui P. Ribeiro,[†] Ticiane P. Sauer,[†,‡] Filipe V. Lopes,[†] Regina F. Moreira,[‡] Carlos A. Grande,*[,†] and Alírio E. Rodrigues[†]

Laboratory of Separation and Reaction Engineering (LSRE), Associate Laboratory LSRE/LCM, Department of Chemical Engineering, Faculty of Engineering, University of Porto, Rua Dr. Roberto Frias, s/n, 4200-465, Porto, Portugal, and Laboratory of Energy and Environment (LEMA), Federal University of Santa Catarina, Florianópolis, Brazil

Biomethane generated from renewable sources can be used as a renewable fuel to achieve ambitious targets for biofuels. The development of adsorption-based technologies for purification of biogas requires knowledge of adsorption equilibria and kinetics of pure gases on a specific adsorbent material. In this work, we have measured adsorption equilibria of CO_2, CH_4, and N_2 at (299, 323, 348, 373, and 423) K over a pressure range between (0 and 700) kPa on a carbon honeycomb monolith. The adsorption capacity of the activated carbon honeycomb monolith was $CO_2 > CH_4 > N_2$. The multisite Langmuir model was employed to fit the data of the pure gases offering the possibility of direct prediction of multicomponent adsorption equilibria. The diffusion of single gases in the microporous structure of the activated carbon honeycomb monolith was studied by diluted breakthrough experiments. The experiments were performed over the same temperature range [(303 to 423) K]. A simplified 1D mathematical model was employed in the description of the adsorption phenomenon. The data reported in this work allows modeling of adsorption processes such as pressure swing adsorption (PSA) and temperature swing adsorption (TSA).

1. Introduction

Biomethane generated from renewable sources can be used as engine fuel. This renewable fuel may also play an important role in an integrated strategy to achieve ambitious targets for biofuels within Europe (25 % of total road transport in 2030) and worldwide. Biomethane can be obtained from anaerobic decomposition of organic matter, and the most important sources are digestors (manure and agro-forest matter) and landfills (municipal solid waste). Biogas composition is strongly dependent on the source and is within (50 to 75) % CH_4, where the main contaminant is carbon dioxide (up to 50 %). The removal of CO_2 from biogas to obtain biomethane with purity above 98 % is the most expensive step in the upgrading. Depending on the extraction method employed in landfills, nitrogen can also be found as a contaminant with contents up to 10 %. Water washing, amine scrubbing, pressure swing adsorption (PSA), and membranes are commercial technologies already available to remove CO_2 from biogas, although it is recognized that the energy consumption of actual technologies can be improved.[1]

Specifically, PSA is employed to remove CO_2 from biogas[2] and also for N_2 rejection from natural gas.[3] Power consumption in PSA technologies can be improved if materials with enhanced adsorption properties are employed. A very interesting property of honeycomb monoliths is that the pressure drop is almost negligible.[4] The use of honeycomb monoliths for adsorption processes is rather new, and only a few applications have been reported for bulk removal of contaminants.[5] Many of the papers employing honeycombs deal with the removal of trace components like VOCs.[6−11]

Recently, intensive wok was performed to identify adsorbents for CO_2 under different operating conditions and streams. Some of the adsorbents are: silicalite,[12] alumina,[13] carbon molecular sieves,[14] zeolites,[15−17] and silica gel.[18] More recently, metal-organic frameworks (MOFs) have revealed extraordinary adsorption capacity for CO_2, being potential adsorbers for this biogas purification.[19,20]

In this work, we report adsorption equilibria and kinetics of pure CO_2, CH_4, and N_2 on an activated carbon honeycomb monolith over wide temperature and pressure ranges. The objective of the work is to provide fundamental data to simulate the behavior of adsorption-based processes with the advantages of employing a honeycomb monolith: very low pressure drop of the process and easiness in the PSA scale-up.

2. Experimental

The adsorbent material used in the study was an activated carbon honeycomb monolith supplied by Mast Carbon (United Kingdom). The honeycomb is a cylinder with a length of 0.1 m and diameter of 0.022 m with 300 parallel square channels.

Scanning electron microscopy (SEM) was performed with a JEOL JSM 6301F (Japan) to determine the dimension of the channels and the thickness of the walls of the honeycomb monolith. A SEM image of the adsorbent can be observed in Figure 1. The channels are very regular with side length between (678 and 710) μm, while the channel walls have a thickness between (447 and 469) μm.

Mercury porosimetry was employed to determine the macroporous structure of the adsorbent. The macropore size distribution of the honeycomb monolith can be observed in Figure 2. It can be observed that an important number of macropores with a diameter of 3.45 μm are present. The density of the material is 989.2 kg·m^{-3}. Adsorption of N_2 at 77 K was also measured. The surface area calculated with the Barrett−

* To whom correspondence should be addressed. Phone: +351 22 508 1618. Fax: +351 22 508 1674. E-mail: cgrande@fe.up.pt.
† University of Porto.
‡ Federal University of Santa Catarina.

10.1021/je800161m CCC: $40.75
Published on Web 09/04/2008

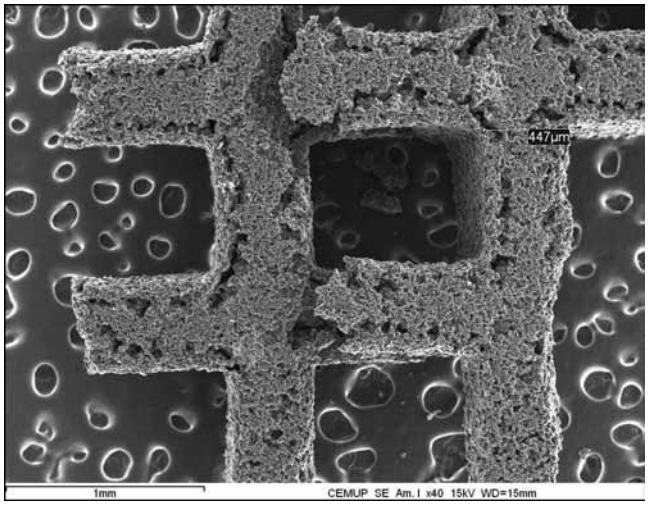

Figure 1. Morphology of the activated carbon honeycomb monolith.

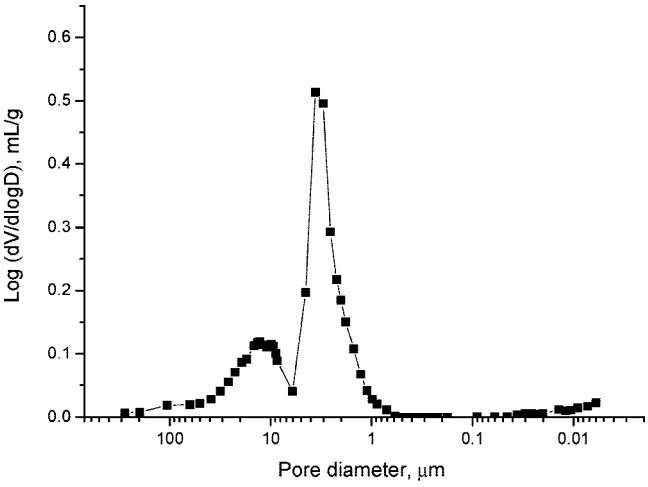

Figure 2. Macropore size distribution of the activated carbon honeycomb monolith.

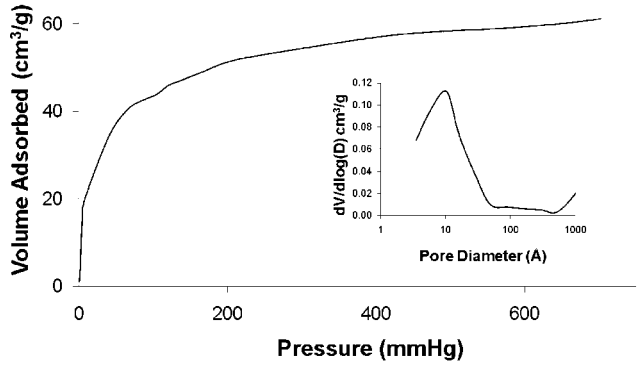

Figure 3. N_2 adsorption isotherm at 77 K and micropore size distribution of the activated carbon honeycomb monolith.

Joiner−Halenda (BJH) method is 483 $m^2 \cdot g^{-1}$. The N_2 isotherm and the micropore size distribution are shown in Figure 3.

Adsorption equilibrium measurements of pure gases were performed in a magnetic suspension microbalance (Rubotherm, Germany) operated in a closed system. Measurements were performed with a cutoff of the adsorbent with approximately 5 g to minimize errors of the measurements, which are already very small (± 0.00002 g). A pressure transducer from (0 to 700) kPa was employed for the measurements (± 0.14 kPa).

Table 1. Breakthrough Curve Experimental Conditions

parameter	value
mass of adsorbent (g)	25.52
bed diameter (cm)	2.2
bed length (cm)	10
bed porosity	0.33
flow rate ($cm^3 \cdot min^{-1}$)	14.60[a]
temperature (K)	303, 323, 348, 373, 423
total pressure (kPa)	101.325
adsorbent density ($kg \cdot m^{-3}$)	989.2
adsorbate molar fraction	0.005

[a] Measured at 296 K and atmospheric pressure

An initial degassing of the sample was carried out under vacuum at 423 K overnight. Regeneration for different experiments was only performed under vacuum at the desired temperature. Isotherms of nitrogen, methane, and carbon dioxide were measured at (299, 323, 348, 373, and 423) K in the range of (0 to 700) kPa. According to several measurements of adsorption and desorption data, we have observed that all the isotherms reported are reversible and can be reproduced.

Kinetics of adsorption (diffusion rates) of pure gases was measured by diluted breakthrough curves of the pure gases diluted in helium. An initial degassing of the sample was performed at 423 K under the flow of helium overnight, while regeneration was only carried out under a flow of helium. The feed had 0.5 % of each adsorbate (CO_2, CH_4, or N_2) mixed with helium (considered as an inert gas). A distance of 2 cm was maintained before the entrance of feed in the honeycomb structure to improve gas distribution over all channels. The external diameter of the honeycomb was covered with a Teflon trap to avoid gas bypassing. The column was placed in a GC oven (CP 3800 Gas Chromatograph - Varian) to control the temperature of each experiment within ± 0.1 K. A four-way valve was employed to switch between feed (adsorbate + helium) and inert gas (helium) for adsorption and desorption measurements, respectively. The breakthrough curves of the three pure gases (CO_2, CH_4, and N_2) were measured in the same temperature range employed in the equilibria measurements [(303 to 423) K] and at atmospheric pressure. The outlet concentration was analyzed by a thermal conductivity detector (TCD). Experimental conditions employed in the measurements are detailed in Table 1.

All gases used in the experiments were supplied by Air Liquide (Portugal) with purities of: CO_2 > 99.998 %, CH_4 > 99.95 %, N_2 > 99.995 %, and He > 99.999 %.

3. Theoretical

Adsorption Equilibrium of Pure Gases. To obtain the absolute amount of gas adsorbed at the different temperatures, buoyancy correction was performed. The experimental value of gas adsorbed in the sample corresponds to the excess amount of gas. The absolute amount adsorbed cannot be obtained directly because it is not possible to measure the density of the adsorbed phase. The method employed for buoyancy corrections was already used for measurements employing these gases in other adsorbents[21] and is based on the assumption that the density of the adsorbed phase can be approximated with the density of the liquid at the boiling point at atmospheric pressure.[22] The data reported in this work correspond to the absolute amount adsorbed.

We have used the multisite Langmuir model[23] to fit the adsorption equilibria of the pure gases and predict the behavior of multicomponent mixtures based on pure component parameters. The multisite Langmuir model assumes that each adsorbate

Table 2. Fitting Parameters of the Langmuir Model and Multisite Langmuir Model

	Langmuir model				multisite Langmuir model			
gas	q_{max} (mol·kg^{-1})	k_0 (kPa^{-1})	$-\Delta H$ (J·mol^{-1})	a	q_{max} (mol·kg^{-1})	k_0 (kPa^{-1})	$-\Delta H$ (J·mol^{-1})	a
CO_2	5.5641	$6.20\cdot10^{-7}$	24016.6	1	7.2162	$3.27\cdot10^{-7}$	25765.9	2.01
CH_4	3.7946	$1.07\cdot10^{-6}$	21267.7	1	5.9380	$5.56\cdot10^{-7}$	22327.1	2.4
N_2	2.9717	$1.76\cdot10^{-6}$	17082.8	1	5.9422	$8.69\cdot10^{-7}$	17220.6	2.5

molecule can occupy more than one site, all of them with equal energies.[24] Neglecting the adsorbate−adsorbate interactions, the model can be expressed as

$$\left(\frac{q_i}{q_{max,i}}\right) = K_i P\left[1-\left(\frac{q_i}{q_{max,i}}\right)\right]^{a_i} \quad (1)$$

where $q_{max,i}$ is the maximum amount adsorbed of component i; a_i is the number of neighboring sites occupied by a molecule of component i; P is the gas pressure; and K_i is the adsorption constant which has an Arrhenius exponential temperature dependence as

$$K_i = K_i^0 \exp\left(-\frac{\Delta H_i}{R_g T}\right) \quad (2)$$

where T is the temperature; R_g is the ideal gas constant; K_i^0 is the adsorption constant of component i at the limit of $T\rightarrow\infty$; and $(-\Delta H_i)$ is the isosteric heat of adsorption of component i at zero coverage. The saturation capacity of each component is imposed by the thermodynamic constraint $a_i q_{max,i}$ = constant.

The multisite Langmuir model is an implicit equation, and in the particular case when $a_i = 1$, the model corresponds to the Langmuir model and can be written as an explicit equation of the form

$$q_i = q_{max,i}\frac{K_i P}{1+K_i P} \quad (3)$$

Both the multisite Langmuir and Langmuir models were fitted to the experimental data using the *fmins* function of the MATLAB 6.0 program (The Mathworks, Inc.).

The adsorption equilibria provide information of the isosteric heat of adsorption, Q_{st}. The isosteric heat corresponds to the energy of adsorption released in an adsorption process and depends on the temperature and surface coverage. The isosteric heat can be determined from a set of isotherms according to the Clapeyron equation

$$Q_{st} = -R_g T^2\left(\frac{\partial \ln P}{\partial T}\right)_q \quad (4)$$

The derivative must be evaluated at constant loadings. In this work, at least three isotherms at different temperatures were employed for the determination of the dependence of isosteric heat with adsorbed concentration.

Adsorption Kinetics of Pure Gases. In this work, we have measured breakthrough curves of gases with a very low partial pressure diluted in helium. With very low concentration of the adsorbate, its isotherm is linear thus avoiding undesired effects of equilibrium nonlinearity in diffusivity determinations. By using a small concentration of adsorbate, the heat generated by adsorption is small and thus temperature is constant. Also, the velocity variations during adsorption are negligible.

The mathematical model employed to determine the diffusion coefficient assumes that the behavior of the monolith can be described by modeling a single channel.[25] An additional simplification was to assume that the velocity in all the channels is the same. Under these assumptions, a simplified model was employed to fit the diffusivity coefficient to the experimental data. The model considers axially dispersed plug flow and only one resistance to diffusion within the walls of the monolith.

The mass balance for component i in the gas phase is given by

$$\frac{\partial C_i}{\partial t} + \left(\frac{1-\varepsilon_c}{\varepsilon_c}\right)\rho_w \frac{\partial \bar{q}_i}{\partial t} = -v_{ch}\frac{\partial C_i}{\partial z} + D_{ax}\left(\frac{\partial^2 C_i}{\partial z^2}\right) \quad (5)$$

where C_i is the gas concentration of component i for a certain position in the axial coordinate z; t is the time; ε_c is the column porosity; ρ_w is the monolith wall density; $\bar{q}_i$ is the average amount adsorbed of component i in the monolith; v_{ch} is the average velocity in the cross-section of each channel of the monolith; and D_{ax} is the axial dispersion coefficient.

The initial and boundary conditions for the mass balance are

$$C_i(t=0) = 0 \quad (6)$$

$$C_i(z=0) = C_{i,feed} \quad (7)$$

$$\left(\frac{\partial C_i}{\partial z}\right)_{(x,y,z=L_c)} = 0 \quad (8)$$

where $C_{i,feed}$ is the concentration of component i in the feed stream and x and y are the Cartesian coordinates of the monolith channel.

Mass transport in the solid phase is expressed by the following equation

$$\frac{\partial \bar{q}_i}{\partial t} = \frac{3D_{s,i}}{l_c^2}(q_i^* - \bar{q}_i) \quad (9)$$

where $D_{s,i}$ is the effective diffusivity in the solid phase; l_c is the corrected wall thickness; and q^* is the adsorbed phase concentration in the equilibrium state. The initial condition is expressed by

$$\bar{q}_i(t=0) = 0 \quad (10)$$

Since the channel geometry is square, we need to make a simplification in the wall thickness (representative dimension for diffusion path) to be introduced in an infinite-slab model. The approximation used in this work is based on the assumption that the corners of the channels are added to the side walls as illustrated by Figure 4. This assumption was already employed[26] as a simplification technique to reduce simulation time. The corrected half-thickness of the wall of a channel, l_c, is given by[26]

$$l_c = l(1 + l/2R_{in}) \quad (11)$$

where l is the wall half-thickness and R_{in} is the half-side of the square channel.

The axial dispersion coefficient was calculated by[11]

$$D_{ax} = D_m + \frac{1}{192}\frac{v_{ch}^2(2R_{in})^2}{D_m} \quad (12)$$

where D_m is the molecular diffusivity.

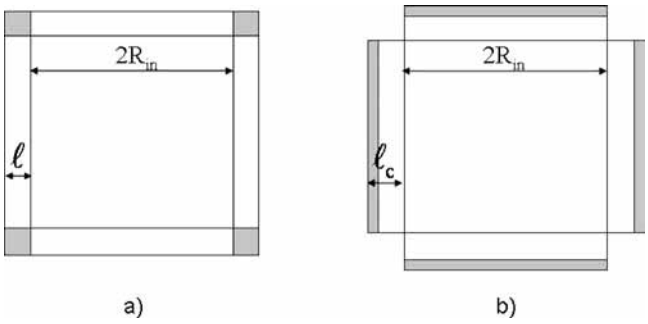

Figure 4. Schematic diagram of (a) one channel of the carbon honeycomb monolith and (b) corrected geometry employed in the simulations.

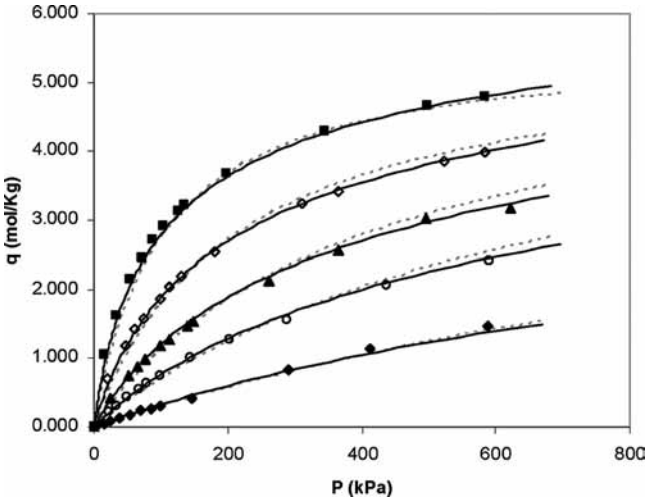

Figure 5. Carbon dioxide adsorption equilibrium on the activated carbon honeycomb monolith at ■, 299 K; ◇, 323 K; ▲, 348 K; ○, 373 K; and ♦, 423 K. The solids lines represent the Nitta model and dotted lines the Langmuir model.

Simulations of the mathematical model presented in this section were performed in gPROMS (PSE, United Kingdom) using orthogonal collocation of finite elements. The objective of using a simplified axially dispersed plug flow (1D) model was to reduce the computation time to provide an easy tool for fast design of adsorption-based processes. The simulations of breakthrough curves do not take more than 20 s in a Pentium IV personal computer ensuring fast simulation of a PSA process.

4. Results and Discussion

Adsorption equilibrium data of CO_2, CH_4, and N_2 are shown in Figures 5, 6, and 7, respectively. It can be observed that CO_2 is more adsorbed than the other gases followed by CH_4, while N_2 is the least adsorbed species. The selectivity toward carbon dioxide decreases when increasing the pressure (see Figure 8). The equilibrium selectivity factor, α, was calculated by

$$\alpha_{ij} = \frac{q_i}{q_j} \tag{13}$$

where q_i and q_j are, respectively, the adsorbed quantity of the most adsorbed species and the adsorbed quantity of the least adsorbed species.

The figures also show the fitting of the Langmuir (dashed lines) and multisite Langmuir models (solid lines). The parameters of the fitting for both models are detailed in Table 2. The thermodynamic restriction of the $a_i q_{\max,i}$ = constant was satisfied in the fitting of the multisite Langmuir model. The accuracy of the fitting of the Langmuir model is not as good as the multisite

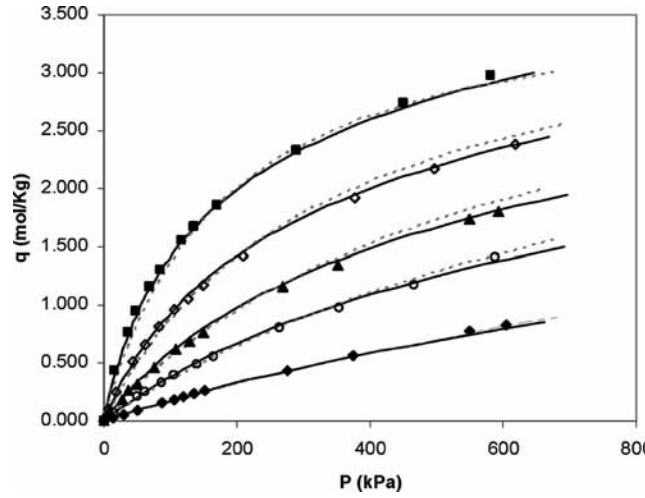

Figure 6. Methane adsorption equilibrium on the activated carbon honeycomb monolith at ■, 299 K; ◇, 323 K; ▲, 348 K; ○, 373 K; and ♦, 423 K. The solids lines represent the Nitta model and dotted lines the Langmuir model.

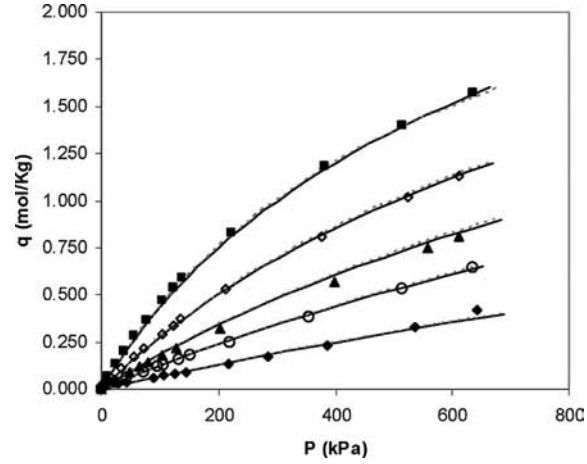

Figure 7. Nitrogen adsorption equilibrium on the activated carbon honeycomb monolith at ■, 299 K; ◇, 323 K; ▲, 348 K; ○, 373 K; and ♦, 423 K. The solids lines represent the Nitta model and dotted lines the Langmuir model.

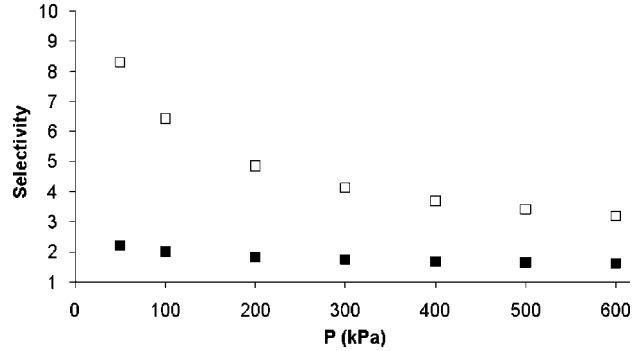

Figure 8. Selectivity of ■, CO_2/CH_4 and □, CO_2/N_2 as a function of pressure at 299 K.

Langmuir, especially for higher pressures, but this model was able to predict the trend of the data. Adsorption and desorption experiments were performed indicating that all the isotherms were reversible.

Isosteric Heats of Adsorption. Variations of the isosteric heat of adsorption for different loadings of adsorbate were calculated with the Clapeyron equation. Figure 9 shows the isosteric heat obtained for each gas as a function of the

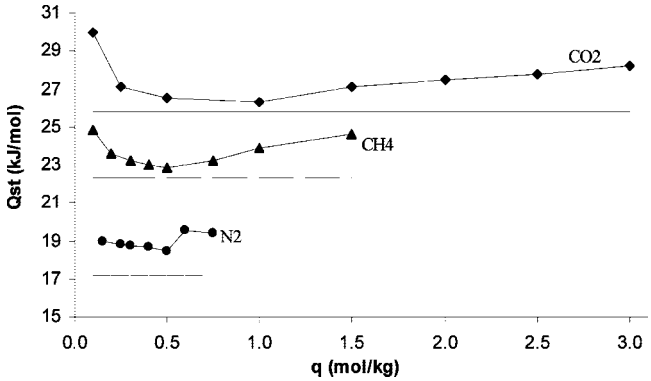

Figure 9. Isosteric heat as a function of loading for ◆, CO_2; ▲, CH_4; and ●, N_2. Values from experimental adsorption equilibrium data. The horizontal lines represent the values obtained from the fitting of the multisite Langmuir model.

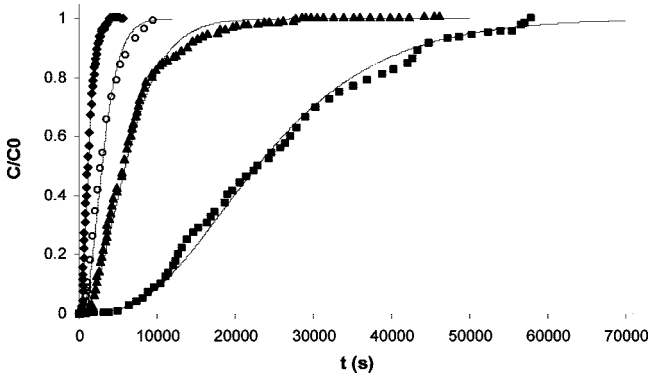

Figure 10. Diluted breakthrough curves of carbon dioxide in the activated carbon honeycomb monolith at ■, 303 K; ▲, 348 K; ○, 373 K; and ♦, 423 K. The solids lines represent the fitting with the theoretical model.

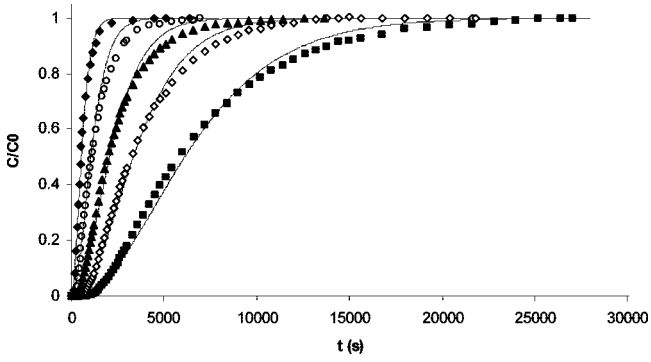

Figure 11. Dilute breakthrough curves of methane in the activated carbon honeycomb monolith at ■, 303 K; ◇, 323 K; ▲, 343 K; ○, 373 K; and ♦, 423 K. The solids lines represent the fitting with the theoretical model.

amount adsorbed. In the plot, we are also showing the heats of adsorption of the multisite Langmuir model which should be constant with loading according to assumptions of a homogeneous surface. The isosteric heat calculated from the experimental data varies for different amounts adsorbed and is slightly higher than the values obtained from the multisite Langmuir model.

Adsorption Kinetics. The diffusion of single gases in the microporous structure of the activated carbon honeycomb monolith was studied by diluted breakthrough experiments. Experimental conditions of the experiments and of the column are reported in Table 1. The breakthrough experiments of CO_2, CH_4, and N_2 are shown in Figures 10, 11, and 12, respectively. The adsorption capacity determined from these

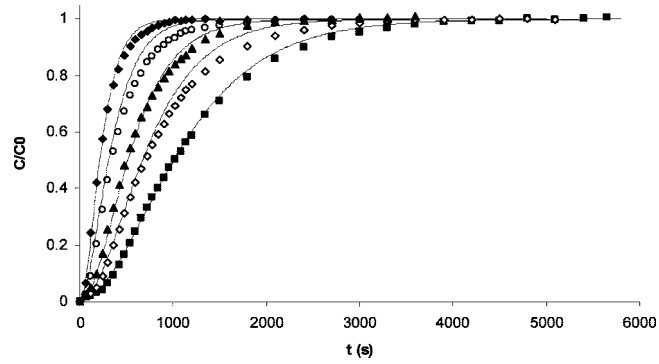

Figure 12. Dilute breakthrough curves of nitrogen in the activated carbon honeycomb monolith at ■, 303 K; ◇, 323 K; ▲, 343 K; ○, 373 K; and ♦, 423 K. The solids lines represent the fitting with the theoretical model.

Table 3. Diffusion Coefficients of CO_2, CH_4, and N_2 in an Activated Carbon Honeycomb Monolith at Temperatures between 303 K and 423 K[a]

gas	T (K)	D_s ($m^2 \cdot s^{-1}$)	D_s^0 ($m^2 \cdot s^{-1}$)	E_a ($kJ \cdot mol^{-1}$)
CO_2	303	$1.15 \cdot 10^{-11}$	$2.28 \cdot 10^{-7}$	25.030
	348	$3.50 \cdot 10^{-11}$		
	373	$7.80 \cdot 10^{-11}$		
	423	$1.85 \cdot 10^{-10}$		
CH_4	303	$3.00 \cdot 10^{-11}$	$7.36 \cdot 10^{-8}$	19.477
	323	$5.50 \cdot 10^{-11}$		
	343	$8.00 \cdot 10^{-11}$		
	373	$1.50 \cdot 10^{-10}$		
	423	$2.70 \cdot 10^{-10}$		
N_2	303	$1.50 \cdot 10^{-10}$	$1.98 \cdot 10^{-8}$	12.156
	323	$2.20 \cdot 10^{-10}$		
	343	$2.90 \cdot 10^{-10}$		
	373	$4.00 \cdot 10^{-10}$		
	423	$6.00 \cdot 10^{-10}$		

[a] Exponential description of diffusion according to $D_s = D_s^0 \exp(-E_a/RT)$.

Table 4. Comparison of Adsorption Capacity Determined from Diluted Breakthrough Curves and from the Multisite Langmuir Model

gas	temperature (K)	$q_{dynamic}$ ($mol \cdot kg^{-1}$)	q_{MSL} ($mol \cdot kg^{-1}$)
CO_2	303	0.0498	0.0326
	348	0.0131	0.0087
	373	0.0066	0.0048
	423	0.0025	0.0018
CH_4	303	0.0143	0.0132
	323	0.0078	0.0081
	343	0.0048	0.0040
	373	0.0024	0.0022
	423	0.0013	0.0010
N_2	303	0.0024	0.0024
	323	0.0016	0.0016
	343	0.0012	0.0013
	373	0.0007	0.0007
	423	0.0005	0.0005

breakthrough curves is reported in Table 4. For comparison purposes, we have also included in this table the calculated amount adsorbed determined from the multisite Langmuir fitting. Some differences may be observed in the case of CO_2 which indicates some differences between the experimental point and the fitting of the multisite Langmuir model at very low pressures.

Diffusivity coefficients were determined by fitting the model to the experimental data. The theoretical model based on a single, lumped resistance proves to fit the experimental data well (see solid lines in Figures 10, 11, and 12). The deviations

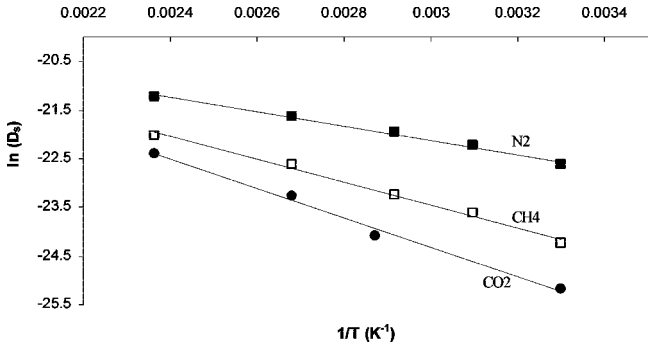

Figure 13. Temperature dependence of diffusivity coefficients of ●, CO_2; □, CH_4; and ■, N_2 in the activated carbon honeycomb monolith between (303 and 423) K.

between theoretical results and experimental data are due to the fact that activated carbon possesses a distribution of pores instead of a single value as considered in the model.

The diffusivity coefficient determined with this lumped model results from a combination of the macropore and micropore diffusivities. An exponential dependence of the solid diffusivity with temperature is shown in Figure 13 for all gases. The exponential dependence of the diffusion coefficient seems to correctly describe the data within the temperature range studied. However, this is not indicative that at higher temperatures the control mechanism for diffusion is within the micropores. Numerical values of diffusion coefficients are reported in Table 3.

The single-gas adsorption equilibrium parameters reported in Table 2 can be used to predict multicomponent adsorption equilibrium behavior. The necessary equations to describe binary or ternary behavior are detailed below for the Langmuir model (eq 14) and for the multisite Langmuir model (eq 15).

The Langmuir isotherm can be extended to multicomponent systems by

$$q_i = \frac{q_{\max,i} K_{\mathrm{eq},i} y_i P}{1 + \sum K_{\mathrm{eq},i} y_i P} \tag{14}$$

where $q_{\max,i}$ is the maximum adsorption capacity of component i; $K_{\mathrm{eq},i}$ is the adsorption constant of component i; y_i is the molar fraction of component i; and P is the equilibrium pressure.

For multicomponent systems, the Nitta multisite Langmuir model equation can be expressed as

$$\frac{q_i}{q_{\max,i}} = K_{\mathrm{eq},i} y_i P \left(1 - \sum \frac{q_i}{q_{\max,i}}\right)^{a_i} \tag{15}$$

where a_i is the number of neighboring sites occupied by component i.

5. Conclusions

Adsorption isotherms of carbon dioxide, methane, and nitrogen on an activated carbon honeycomb monolith were measured at five different temperatures ranging from (299 to 423) K in a pressure range from (0 to 700) kPa. The results were correlated with the Langmuir and multisite Langmuir models. The fitting of the multisite Langmuir model is better.

Diffusion of the gases through the microporous structure of the monoliths was studied by diluted breakthrough curves of pure gases in the same temperature range. A mathematical model using one lumped resistance was employed to determine diffusivity coefficients from experimental data. The model proved to be accurate in the description of the kinetics of adsorption of the pure gases. This model employed allows a significant reduction in computing time required when compared with more complex models.

The data provided in this work allows modeling of adsorption processes such as pressure swing adsorption (PSA) and temperature swing adsorption (TSA) for separation of this ternary mixture of gases using an activated carbon honeycomb monolith.

Literature Cited

(1) Biofuels Research Advisory Council. Biofuels in the European Union. A Vision for 2030 and beyond, 2006.

(2) Carbotech - Products for People and Environment. Commercial brochure available at: http://www.carbotech.de/en/general_information.php (accessed 2008/02/28).

(3) Kuznicki, S. M.; Bell, B. A.; Petrovic, I.; Desai, B. T. Small-Pored Crystalline Titanium Molecular Sieve Zeolites and Their Use in Gas Separation Processes. U. S. Patent 6,068,682. 2000.

(4) Li, Y. Y.; Perera, S. P.; Crittenden, B. D. Zeolite monoliths for air separation, part 2: oxygen enrichment, pressure drop and pressurization. *Trans. I ChemE* **1998**, 76.

(5) Kopaygorodsky, E. M.; Guliants, V. V.; Krantz, W. B. Predictive dynamic model of single-stage ultra-rapid pressure swing adsorption. *AIChE J.* **2004**, *50*, 5.

(6) Gadkaree, K. P. System and method for adsorbing contaminants and regenerating the adsorber. US Patent 5,658,372. 1997.

(7) Lee, L. Y.; Perera, S. P.; Crittenden, B. D.; Kolaczkowski, S. T. Manufacture and characterization of silicate monoliths. *Adv. Sci. Technol.* **2000**, *18*, 147–170.

(8) Kim, D. J.; Kim, J. W.; Yie, J. E.; Moon, H. Temperature-programmed adsorption and characteristics of honeycomb hydrocarbon adsorbers. *Ind. Eng. Chem. Res.* **2002**, *41*, 6589–6592.

(9) Yu, F. D.; Luo, L. A.; Grevillot, G. Adsorption isotherms of VOCs onto an activated carbon monolith: experimental measurement and correlation with different models. *J. Chem. Eng. Data* **2002**, *47*, 467–473.

(10) Yates, M.; Blanco, J.; Martin-Luengo, M. A.; Martin, M. P. Vapour adsorption capacity of controlled porosity honeycomb monoliths. *Microporous Mesoporous Mater.* **2003**, *65*, 219–231.

(11) Valdés-Solís, T.; Linders, M. J. G.; Kapteijn, F.; Marbán, G.; Fuertes, A. B. Adsorption and breakthrough performance of carbon-coated ceramic monoliths at low concentration of n-butane. *Chem. Eng. Sci.* **2004**, *59*, 2791–2800.

(12) Delgado, J. A.; Uguina, M. A.; Soleto, J. L.; Ruíz, B. Fixed-bed adsorption of carbon dioxide-helium, nitrogen-helium and carbon dioxide-nitrogen mixtures onto silicate pellets. *Sep. Purif. Technol.* **2006**, *49*, 91–100.

(13) Gomes, V. G.; Yee, W. K. Pressure swing adsorption for carbon dioxide sequestration from exhaust gases. *Sep. Purif. Technol.* **2002**, *28*, 161–171.

(14) Cavenati, S.; Grande, C. A.; Rodrigues, A. E. Upgrade of methane from landfill gas by pressure swing adsorption. *Energy Fuels* **2005**, *19*, 2545–2555.

(15) Himeno, S.; Tomita, T.; Suzuki, K.; Yoshida, S. Characterization and selectivity for methane and carbon dioxide adsorption on the all-silica DD3R zeolite. *Microporous Mesoporous Mater.* **2007**, *98*, 62–69.

(16) Cavenati, S.; Grande, C. A.; Rodrigues, A. E. Adsorption equilibrium of methane, carbon dioxide and nitrogen on zeolite 13X at high pressures. *J. Chem. Eng. Data* **2004**, *49*, 1095–1101.

(17) Harlick, P. J. E.; Tezel, F. H. An experimental adsorbent screening study for CO_2 removal from N_2. *Microporous Mesoporous Mater.* **2004**, *76*, 71–79.

(18) Knowles, G. P.; Graham, J. V.; Delaney, S. W.; Chaffee, A. L. Aminopropyl-functionalized mesoporous silicas as CO_2 adsorbents. *Fuel Process. Technol.* **2005**, *86*, 1435–1448.

(19) Skoulidas, A. I.; Sholl, D. S. Self-diffusion and transport diffusion of light gases in metal-organic framework materials assessed using molecular dynamics simulations. *J. Phys. Chem. B* **2005**, *109* (33), 15760–15768.

(20) Keskin, S.; Sholl, D. S. Screening metal-organic framework materials for membrane-based methane/carbon dioxide separations. *J. Phys. Chem. C* **2007**, *111* (38), 14055–14059.

(21) Cavenati, S.; Grande, C. A.; Rodrigues, A. E. Separation of CH_4/CO_2/N_2 mixtures by layered pressure swing adsorption for upgrade of natural gas. *Chem. Eng. Sci.* **2005**, *61*, 3893–3906.

(22) Dreisbach, F.; Staudt, R.; Keller, J. U. High Pressure Adsorption Data of Methane, Nitrogen, Carbon Dioxide and their Binary and Ternary Mixtures on Activated Carbon. *Adsorption* **1999**, *5*, 215–227.

(23) Nitta, T.; Shigetomi, T.; Kuro-Oka, M.; Katayama, T. An adsorption isotherm of multi-site occupancy model for homogeneous surface. *J. Chem. Eng. Jpn.* **2006**, *17*, 39–45.

(24) Do, D. D. *Adsorption analysis: equilibria and kinetics*; Imperial College Press: London, 1984.

(25) Young, L. C.; Finlayson, B. A. .Mathematical modeling of the monolith converter. *Adv. Chem. Ser.* **1974**, *13*, 629–643.

(26) Ahn, H.; Brandani, S. Dynamics of carbon dioxide breakthrough in a carbon monolith over a wide concentration range. *Adsorption* **2005**, *11*, 473–477.

Received for review March 06, 2008. Accepted July 25, 2008. The authors would like to thank the Foundation for Science and Technology (FCT) through the project PTDC/EQU-EQU/65541/2006 and GRICES/CAPES 139/05, for financial support.

JE800161M